

## **Supplementary Information**

Structural and kinetic insights into stimulation of RppH-dependent RNA degradation by  
the metabolic enzyme DapF

Ang Gao<sup>1</sup>, Nikita Vasilyev<sup>1</sup>, Daniel J. Luciano<sup>2,3</sup>, Rose Levenson-Palmer<sup>2,3</sup>, Jamie Richards<sup>2,3</sup>,  
William M. Marsiglia<sup>4</sup>, Nathaniel J. Traaseth<sup>4</sup>, Joel G. Belasco<sup>2,3</sup> and Alexander Serganov<sup>1,\*</sup>

<sup>1</sup> Department of Biochemistry and Molecular Pharmacology,

New York University School of Medicine, 550 First Avenue, New York, NY 10016, USA;

<sup>2</sup> Kimmel Center for Biology and Medicine at the Skirball Institute and <sup>3</sup> Department of Microbiology,  
New York University School of Medicine

540 First Avenue, New York, NY 10016, USA

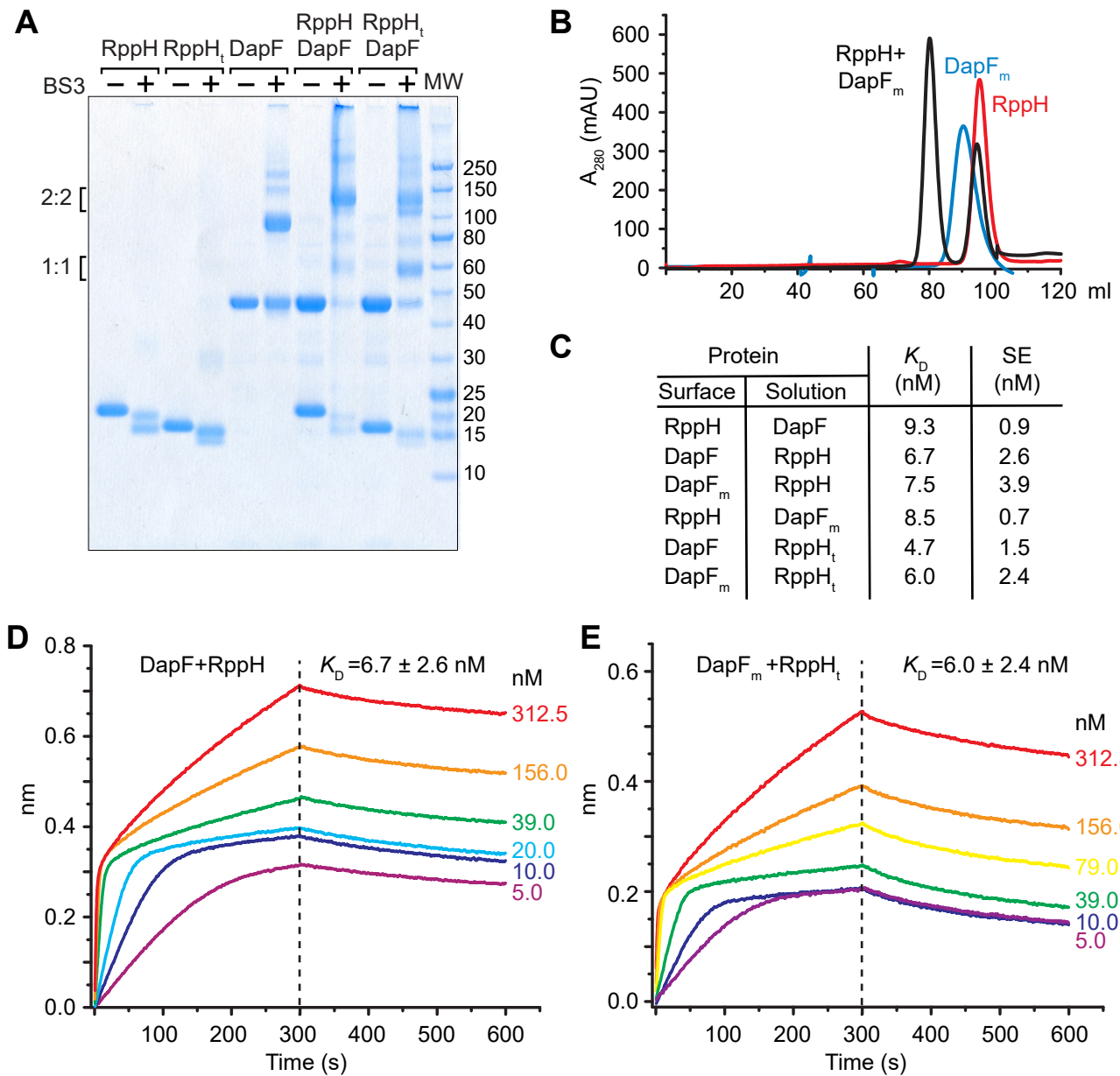
<sup>4</sup> Department of Chemistry, New York University, 100 Washington Square East,  
New York, NY 10003, USA

**Table S1. Data Collection and Refinement Statistics**

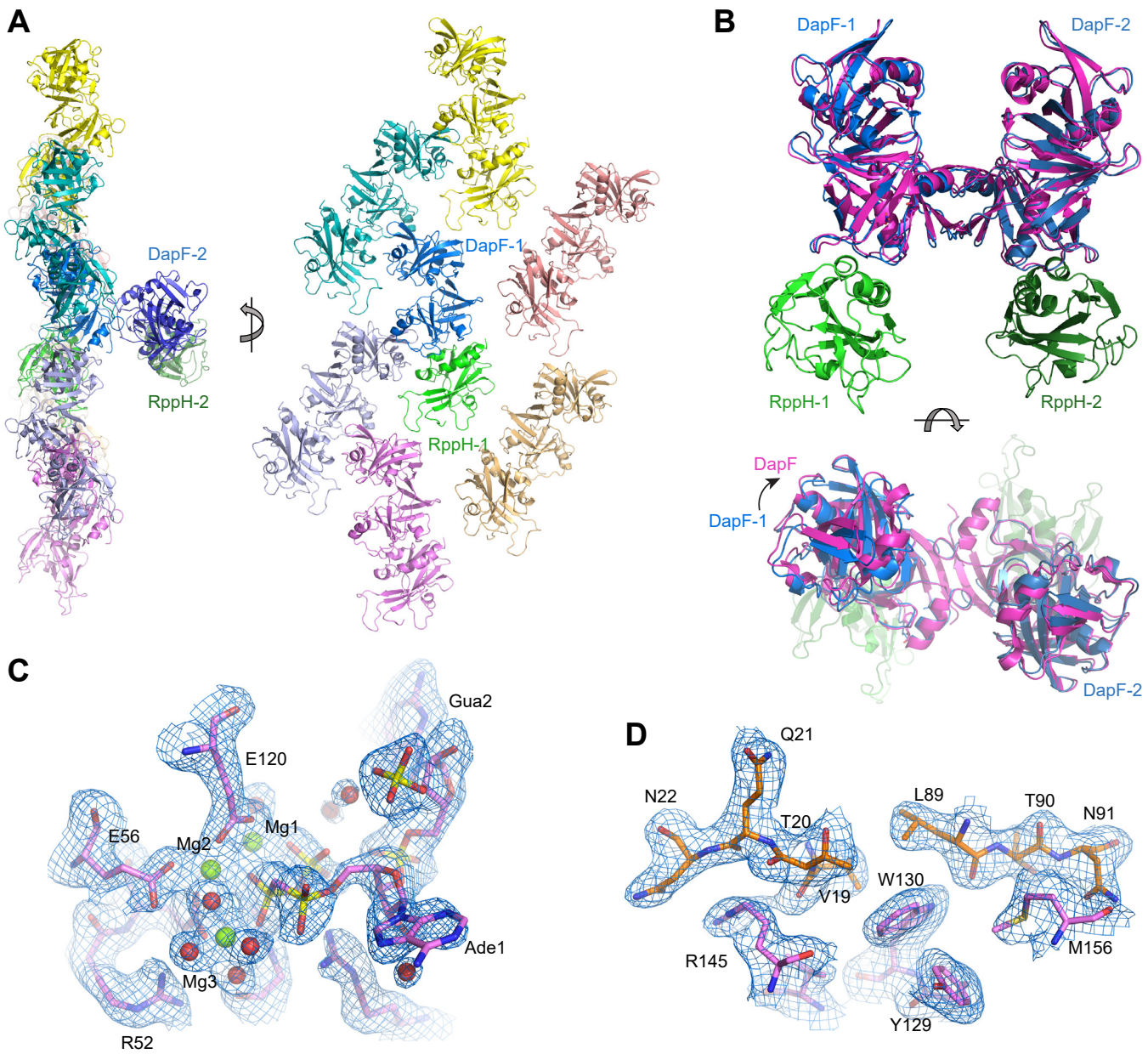
Dataset	RppH-DapF	RppH <sub>t</sub> -DapF <sub>m</sub>	RppH <sub>t</sub> -RNA-DapF <sub>m</sub>
<b>Data collection</b>			
Beam line	APS-24-ID-C	APS-24-ID-C	APS-24-ID-C
Wavelength	0.9793	0.9791	0.9791
Space group	P 4 <sub>1</sub> 2 <sub>1</sub> 2	C 222 <sub>1</sub>	C 222 <sub>1</sub>
Unit Cell			
a, b, c (Å)	85.8, 85.8, 177.4	161.4, 192.3, 50.7	160.6, 192.0, 51.2
Resolution (Å)	85.81-3.06 (3.27-3.06) <sup>a</sup>	123.65-2.15 (2.21-2.15)	123.20-1.81 (1.85-1.81)
R <sub>merge</sub> <sup>b</sup>	0.155 (1.076)	0.049 (1.557)	0.037 (0.989)
C <sup>1/2</sup>	0.995 (0.691)	0.999 (0.331)	0.998 (0.402)
I/σ(I)	13.9 (1.8)	15.2 (1.0)	12.6 (1.0)
Completeness (%)	99.3 (98.9)	99.1 (96.5)	97.1 (81.0)
Redundancy	6.9 (7.3)	4.4 (4.3)	2.9 (2.4)
No. of unique reflections	13,057 (2,296)	43,134 (3,423)	70,344 (3,453)
<b>Refinement</b>			
Resolution (Å)	20-3.06	123.65-2.15	123.20-1.81
R <sub>work</sub> /R <sub>free</sub> (%)	18.7/26.4	21.3/23.4	19.9/22.0
No. of atoms			
Protein	3,440	3,440	3,444
RNA	-	-	58
Water	8	72	288
Ion	13	2	8
Average B factor (Å <sup>2</sup> )			
Protein	98.7	66.8	48.0
RNA	-	-	51.0
Water	68.0	59.0	51.4
Ion	114.3	71.5	50.2
R.m.s. deviations			
Bond lengths (Å)	0.009	0.008	0.008
Bond angles (°)	1.074	1.051	1.036
Ramachandran analysis			
Favored (%)	92.3	95.6	98.4
Outliers (%)	0	0	0
Estimated error <sup>c</sup>	0.45	0.32	0.26

<sup>a</sup> Highest resolution shell (in Å) shown in parentheses.<sup>b</sup> R<sub>merge</sub>= $\sum_{hkl} \sum_{i=1}^n |I_i(hkl) - \bar{I}(hkl)| / \sum_{hkl} \sum_{i=1}^n I_i(hkl)$ , where  $I_i(hkl)$  is the  $i$ th observation of reflection  $hkl$  and  $\bar{I}(hkl)$  is the weighted average intensity for all  $i$  observations of reflection  $hkl$ .<sup>c</sup> Estimated coordinate error based on maximum likelihood was calculated by Phenix.refine.

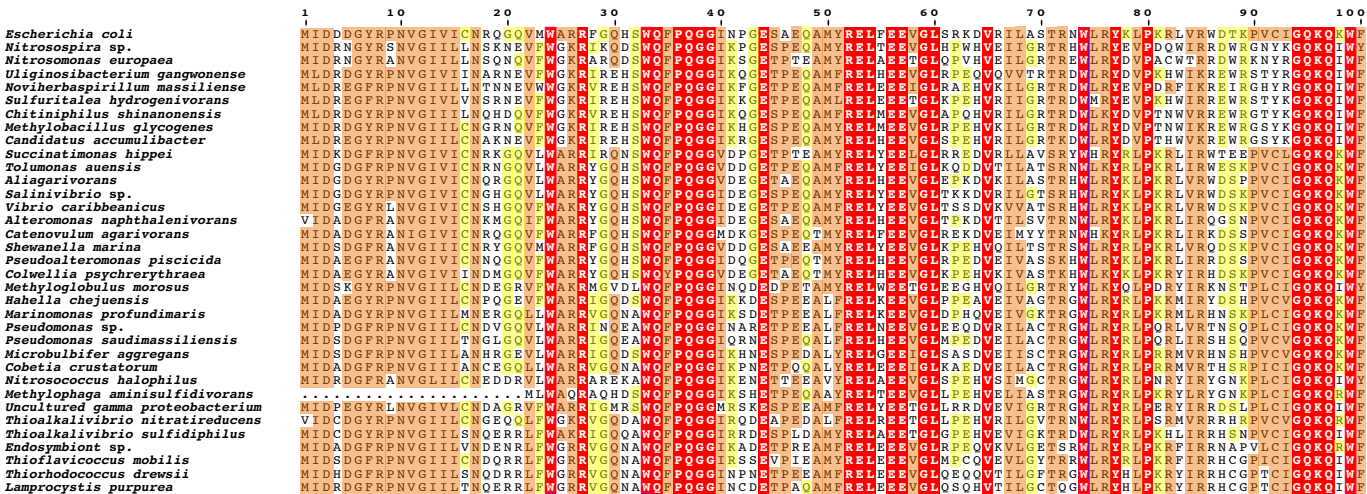
## Supplementary Figures



**Figure S1.** Stoichiometry of the RppH-DapF complex. (A), BS3 crosslinking and SDS-polyacrylamide gel electrophoresis of RppH-DapF complexes using His<sub>6</sub>-SUMO-tagged DapF and full-length or truncated forms of RppH. Double bands observed for crosslinked RppH likely correspond to species with different intramolecular crosslinks. (B), SEC analysis of the RppH-DapF<sub>m</sub> heterodimer (black line), RppH (red line), and dimeric DapF (blue line). RppH was added in excess to DapF to ensure complex formation. The RppH-DapF<sub>m</sub> peak at 80 mL corresponds to a complex with 1:1 stoichiometry, in contrast to the 2:2 stoichiometry of the wild-type RppH-DapF complex, which would elute at 70 mL. (C), Dissociation constants of RppH-DapF complexes, as determined by bio-layer interferometry (BLI).  $K_D$  values are averages of several experiments in which the concentration of the protein in solution was varied. SE, standard error. “Surface” and “solution” identify the immobilized protein and the protein in solution, respectively. (D-E), Association and dissociation curves for representative BLI experiments with RppH and DapF (D) or DapF<sub>m</sub> and RppH<sub>t</sub> (E). The first protein named in each panel title was immobilized. Concentrations of the protein in solution (in nM) are indicated next to each curve.



**Figure S2.** Crystal structure of the RppH-DapF complex. **(A)**, Crystal packing interactions in the crystal of the dimeric RppH-DapF complex. Views show symmetry-related molecules located  $<4\text{ \AA}$  from the base molecules RppH-1 (green) and DapF-1 (blue). The view on the left highlights dimerization of DapF-1 with DapF-2 (dark blue); in this view, the light blue and teal molecules have been omitted for clarity. The view on the right shows other molecules interacting with RppH-1 and DapF-1; in this view, the RppH-2 and DapF-2 molecules have been omitted for clarity. **(B)**, All-atom superposition of the structure of the dimeric RppH-DapF complex on the structure of the *E. coli* DapF-DapF dimer (magenta) (30). Note the similarity of DapF in the two structures and the small clockwise rotation of the C-terminal domains of DapF relative to the central regions of the N-terminal domains in the DapF-DapF complex (bottom panel). **(C and D)**, Fragments of simulated annealing composite omit maps (blue mesh), calculated by PHENIX (24) and contoured at  $1\sigma$  level, with refined structural models for key regions of the structures. **(C)** shows the catalytic site of RppH bound to ppcpAGU RNA (both in violet) from the  $1.8\text{-\AA}$  resolution RppH<sub>t</sub>-ppcpAGU-DapF<sub>m</sub> structure. Mg<sup>2+</sup> cations and water molecules are depicted by green and red spheres, respectively. **(D)** shows the interface between RppH (in violet) and DapF (in orange) from the  $2.1\text{-\AA}$  resolution RppH<sub>t</sub>-DapF<sub>m</sub> structure.

**A**

B

